Heliyon 10 (2024) e28079

Contents lists available at ScienceDirect

Heliyon

journal homepage: www.cell.com/heliyon

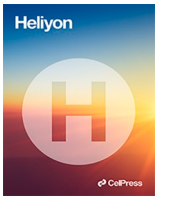

Research article

Preparation, characterization, electrical conductivity, and life cycle assessment of carbon nanofibers-reinforced Ecuadorian natural zeolite-based geopolymer composites

Adriana Alvarado [a], Haci Baykara [b,c,*], Ariel Riofrio [c,d], Mauricio Cornejo [b,c], Wilson Merchan-Merchan [e]

[a] Bert S. Turner Dept. of Construction Management, Louisiana State University, Baton Rouge, LA, 70803, United States
[b] Facultad de Ingeniería Mecánica y Ciencias de la Producción, Escuela Superior Politécnica de Litoral, ESPOL, Campus Gustavo Galindo Km 30.5 Vía Perimetral, Guayaquil, Ecuador
[c] Center of Nanotechnology Research and Development (CIDNA), Escuela Superior Politécnica de Litoral, ESPOL, Campus Gustavo Galindo Km 30.5 Vía Perimetral, Guayaquil, Ecuador
[d] Department of Civil and Environmental Engineering, The Hong Kong University of Science and Technology, Hong Kong SAR, Hong Kong
[e] School of Aerospace and Mechanical Engineering, University of Oklahoma, Norman, OK, 73019, United States

ARTICLE INFO

Keywords:
Carbon nanofiber
Geopolymer composite
Life cycle assessment
Electrical conductivity
Compressive strength

ABSTRACT

Geopolymers are inorganic crosslinked polymers with much less carbon footprint than ordinary Portland cement. Geopolymers and geopolymer-based materials have superior mechanical and durability properties with extreme thermal and chemical resistance. Carbon nano- or microfibers-reinforced geopolymers show potential properties such as electric conductivity, enhanced mechanical and thermal stability, and multi-functionality. This study evaluated the effect of incorporating carbon nanofibers in natural zeolite-based geopolymers and their impact on the mechanical, thermal, and electric conductivity of yielded geopolymer composites. Additionally, a life cycle assessment for 1 m^3 geopolymer and its carbon fiber reinforced geopolymers' production has been conducted to evaluate the environmental impact of the processes.

1. Introduction

There are several challenges that the cement industry is facing, such as the environmental burden from carbon emissions or the limited reserves of limestones [1]. The cement industry is one of the highest contributors to global warming [2]. For this reason, several actions have been considered to address the high volumes of CO_2 emitted each year [3]. One alternative is to develop materials that can significantly decrease the release of gases that contribute to global warming and still maintain mechanical properties similar to or better than OPC. Geopolymer concrete provides a sustainable solution that may reduce up to 80% of the total carbon emissions [4]. Geopolymers are inorganic polymers made of aluminosilicates and have amorphous structures with excellent mechanical properties that are potential alternative replacement materials for OPC [75].

Geopolymers can be prepared via a reaction between an aluminosilicate feedstock and different ratios of alkali hydroxides (NaOH

* Corresponding author. Facultad de Ingeniería Mecánica y Ciencias de la Producción, Escuela Superior Politécnica de Litoral, ESPOL, Campus Gustavo Galindo Km 30.5 Vía Perimetral, Guayaquil, Ecuador.
E-mail address: hbaykara@espol.edu.ec (H. Baykara).

https://doi.org/10.1016/j.heliyon.2024.e28079
Received 12 October 2023; Received in revised form 21 January 2024; Accepted 12 March 2024
Available online 13 March 2024

or KOH) and an alkali silicate [5], which produces an aluminosilicate gel that acts as a binder [6]. Different concentrations of hydroxide and silicate have been studied for different aluminosilicate sources like zeolite, fly ash, and metakaolin [7–10]. Geopolymers require temperature curing to facilitate the reaction [11,12]. The tetrahedral network formed between silicon and aluminum through oxygen bridges during the reaction [13] gives strength to the geopolymer. Geopolymerization of fly ash and metakaolin has been studied for their potential use as substitutes for Portland cement [14–16], since the geopolymer cement production lowers the quantities of CO_2 gas emissions, thus becoming a green cement [17].

There is a growing interest in reinforced geopolymers to enhance their properties [18,19]. One reinforcement material currently being researched is Multiwalled Carbon nanotubes (MCNTs) which are shaped by the rolling of graphene sheets into a cylindrical, hollowed structure. CNTs have reinforced composite matrices [20], which are being employed in the aerospace and automotive industries [21]. On the other hand, carbon nanofibers (CNFs) regularly show a truncated cone-shaped, with numerous stacked layers adjusted along the fiber pivot, including receptive chemical borders on both the interior and exterior of the fiber's surfaces [22]. These materials are convenient as additives since they can improve thermal conductivity [23], reduce bulk resistivity [24], and act as reinforcement in composites like polymers [22,25,26]. CNFs have also been studied as cement reinforcement revealing positive effects on mechanical properties that are ideal for reducing carbon footprint [27]. However, only a few studies have evaluated the effect of CNTs [11,28,29] or CNFs [30,31] in geopolymers. Mechanical properties of geopolymeric materials have been enhanced by the incorporation of CNTs and CNFs inside their matrix. For instance, tensile, compressive, and flexural strengths of the CNF or CNT-reinforced geopolymer samples showed an improvement by 80%, 5–35%, and 9–35%, respectively [10,31–33]. The introduction of CNFs/CNTs can enhance the geopolymer material's mechanical properties and durability while maintaining the geopolymer composites' environmental profile. This can provide a longer-lasting, more sustainable option for industries and applications that rely on these materials. Since geopolymer matrices have amorphous structures with tetrahedral silicate and aluminate units [34], incorporating conductive fillers, such as carbon-based fillers, can offer a new research path to developing innovative building materials with electrochemical sensing, self-sensing concrete, and energy storage applications [35], opening the door for this material to possibly revolutionize energy storage in buildings, roadways, and urban infrastructure [34].

The primary objective of this study is to prepare a geopolymer composite with different CNF concentrations (0–32 wt%) and evaluate its mechanical andelectrical conductivity properties and environmental impacts. In this sense, the paper first presents the preparation process for the geopolymer composites, followed by a comprehensive examination of the mechanical properties and chemical/physical characteristics of the composites, and performs a thorough LCA to evaluate the effect of adding CNFs to a geopolymer matrix [36,37].

2. Materials and methods

2.1. Materials

Natural zeolite was obtained from Zeonatec S.A with an average particle size of ~146 μm (see Fig. 1) and mineral composition of 15.8% quartz, 15% mordenite, 14.1% illite, 5.1 % anorthite, and 49.5% amorphous (See Fig. S1 in the Supplementary Information File). The FTIR spectrum of the zeolite-rich tuff can also be seen in Fig. S2 (in the Supplementary Information File). Sodium hydroxide NaOH (reagent grade, ≥98%, pellets, anhydrous) and sodium silicate ($SiO/Na_2O = 3.4$, Na_2O 7.5–8.5%, and SiO_2 25.5–28.5%, density 1.296–1.396 g/mL) were purchased from Merk. Another sodium silicate solution ($SiO_2/Na_2O = 2.4$, Na_2O 13.27 %, and SiO_2 31.85%, density 1.53 g/mL) was obtained from Proquiandinos S.A. The CNFs used in this study are from Pyrograf-III from Pyrograf Products; the FTIR spectrum of the CNF used in this study can be seen in Fig. S3 (in the Supplementary Information File). These CNFs have a diameter between 100 nm and 150 nm and a length estimated at 100 μm. The CNFs used represent a homogenous mix of CNFs produced by pyrolytically stripping (PR-19-XT-PS and PR-24-XT-PS) and heat-treating (PR-19-XT-LHT).

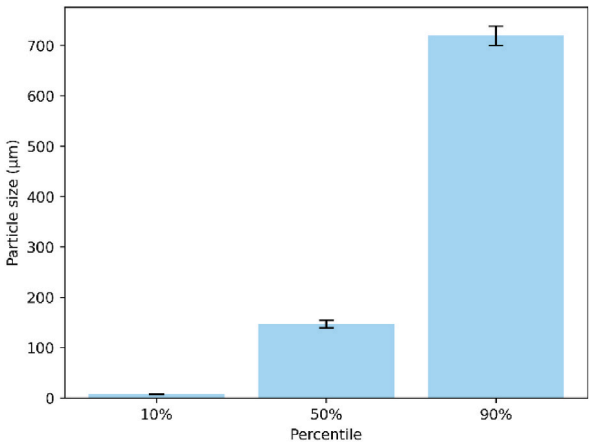

Fig. 1. Particle size distribution for the natural zeolite.

The geopolymer-CNFs reinforced composite was made by varying the sodium silicate. Eight different mixes were prepared with the following codes G0, G1, G2, and G3 (SiO_2/Na_2O ratios of 3.4), and G0*, G1*, G2*, and G3* (SiO_2/Na_2O ratios of 2.4). The quantities used for the different geopolymer composite samples are detailed in Table 1.

Additionally, Fig. 1 presents the particle size distribution of the natural zeolite-rich ruffs used for the geopolymer preparation. As seen in the figure, 90% of the particles have a size of less than 750 μm.

2.2. Geopolymer preparation

First, the sodium hydroxide pellets were weighed and added to ionized water to form the NaOH 10 M; since the process is exothermic, the sodium hydroxide solution was cooled down to room temperature for 8 h. Then, the activator solution was made by mixing the sodium silicate and the sodium hydroxide solutions.

CNFs were dispersed in the activator solution using an adaptation of the method proposed by Saafi et al. [11]. The activator solution was added to the CNFs; then the mix was manually agitated for 5 min, and immediately, it was sonicated for 25 min at 4000J approx. (56 Watts) with the ultrasonic processor GEX 130 PB (see Fig. S4 in the Supplementary Information File). Adding nanomaterials to the activator solution before mixing them into the paste helps prevent them from clumping together [38].

The zeolite was weighted for G0, G1, G2, and G3 geopolymers, and the CNFs-activator solution was added to the zeolite and mixed. The wet geopolymer paste was poured into 50 x 50 × 50 mm cubic molds in a moist and closed environment [39]. After 24 h of casting, the cubes were demolded and cured at room temperature until testing. Fig. 2 shows the systematic scheme for CNF-reinforced geopolymers' composite preparation, and Table 1 shows the elements and quantities used for the design of the geopolymers.

The geopolymer samples were aged for an additional 83 days (see Fig. 3). The same treatment was followed for G0*, G1*, G2*, and G3* geopolymers, the same treatment was followed, but the geopolymer paste was molded into 50 x 50 × 10 mm containers for 30 days. Bulk electrical resistivity testing was carried out for G0, G1, G2, G3, G0*, G1*, G2* and G3* samples.

2.3. Life cycle assessment (LCA)

The LCA in this study aims to evaluate the impacts of the production of zeolite-based and carbon nanofibers (CNFs) reinforced geopolymer composite. The scope of the evaluation will fundamentally consider the life cycle stages included within the extraction and production of the geopolymer CNF composite. The functional unit chosen for the system is 1 m^3 of geopolymer CNF composite. The evaluation will envelop the natural impacts related to asset extraction, fabric handling, and fabricating of the life stages.

The mixes analyzed were conventional GP binder (G0), GP binder with 0.07% CNF (G1), GP binder with 0.2% CNF (G2), and GP binder with 0.32% CNF (G3). In addition, the source of nanocarbon fiber was analyzed to evaluate the best option for nanocarbon fiber production. Three sources were assessed: acetonitrile, benzene, and toluene. The mixes considered the reagents, materials, and energy. The LCA analysis was performed using SimaPro v9.3.0.3 [40] software under the ISO 14040 norm [41]. The system boundary for the LCA can be seen in Fig. 4.

2.4. Life-cycle inventory

The data was assessed following the specification of each mix design presented in detail under the method section. The Ecoinvent dataset v3.7.1 [42] was used to model materials and energy in the inventories. The zeolite in powder form, sodium silicate (without water in 37% concentration), sodium hydroxide (without water in 50% solution), and steam in the factory. The electricity requirement for the process was based on the data for the matrix of Ecuador in the year 2018 [43].

The nanocarbon fibers production and their environmental impact are based on literature for the different evaluated sources and preparation approaches. Literature shows various options and processes for producing nanocarbon fibers, nanotubes, etc. For this analysis, the carbon vapor deposition process was selected using three different sources following the inventory data from Temizel-Sekeryan et al. [44] which is related to single and multi-wall carbon nanotubes (MWCNT). This inventory can also be used for simpler fibers because the main separators between the fibers and tubes are quality parameters such as diameters and dimensional structure.

Table 1
Mixing design for geopolymer preparation.

Specification	Unit	G0	G0*	G1	G1*	G2	G2*	G3	G3*
Na_2O/SiO_2	**%/%**	3.4	2.4	3.4	2.4	3.4	2.4	3.4	2.4
$Na_2O{\cdot}SiO_2$/NaOH sol. ratio	**V/V**	3	3	3	3	3	3	3	3
CNF/Zeolite ratio	**(g/g)**	0	0	0.001	0.001	0.003	0.003	0.005	0.005
CNF wt.%		0	0	0.07	0.07	0.20	0.20	0.32	0.32
Activator/zeolite ratio	**(mL/g)**	0.4	0.4	0.4	0.4	0.42	0.4	0.44	0.4
Zeolite	**(g)**	600	600	600	600	600	600	600	600
Activator	**(mL)**	240	240	240	240	250	240	260	240
NaOH 10M	**(mL)**	60	60	60	60	60	60	60	60
$Na_2O{\cdot}SiO_2$	**(mL)**	180	180	180	180	180	180	180	180
CNF	**(g)**	0	0	0.6	0.6	1.8	1.8	3	3

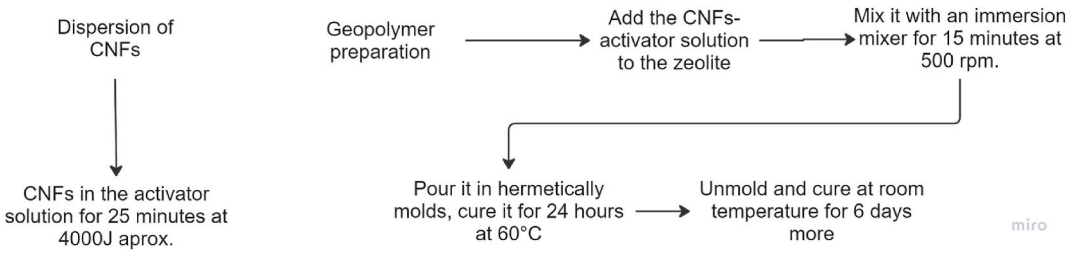

Fig. 2. General diagram for geopolymer and its CNF composites' preparation.

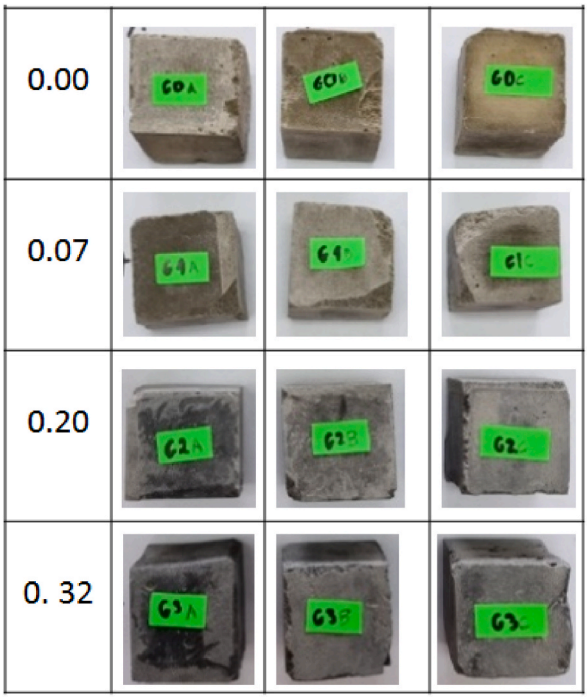

Fig. 3. Photographs of the geopolymer sample cubes prepared with and without CNFs.

2.5. Impact assessment method

The method used to convert data from the inventory to the impact indicator was ReCiPe Midpoint H [45,46] for the geopolymer cement mixes. This impact indicator is characteristic of providing 18 different impact indicators. However, the study will focus on climate change, particulate matter formation, ozone formation, and terrestrial acidification indicators as the priority group to evaluate based on the work of Feng et al. [47] that demonstrated how to prioritize the indicators in an LCA system into two categories for assessing construction materials sustainability. In addition, for the CNFs/CNTs production, the ecotoxicity and human toxicity indicators were evaluated due to the potential impact that some of the raw materials can have on the environment and the human health.

2.6. Characterization methods

Simultaneous thermogravimetric analysis (TGA) and differential scanning calorimetry (DSC) with a heating rate of 10 °C/min, Fourier transformed-infrared spectrophotometry, and X-ray diffraction analyses were conducted according to Ulloa et al. [8] to characterize the various properties of zeolite-based geopolymers and their CNF-reinforced composites.

2.7. Tests methods

The bulk density measurements of the geopolymer samples of G0, G1, G2, and G3 were conducted closely following the methods and procedures by Jittabut et al. [48] at 83 days of curation. The compressive strength test was conducted according to ASTM C109/C109 M-16a [39] norm. This property of all samples was determined using a UHF-500KNX model SHIMADZU Universal Testing

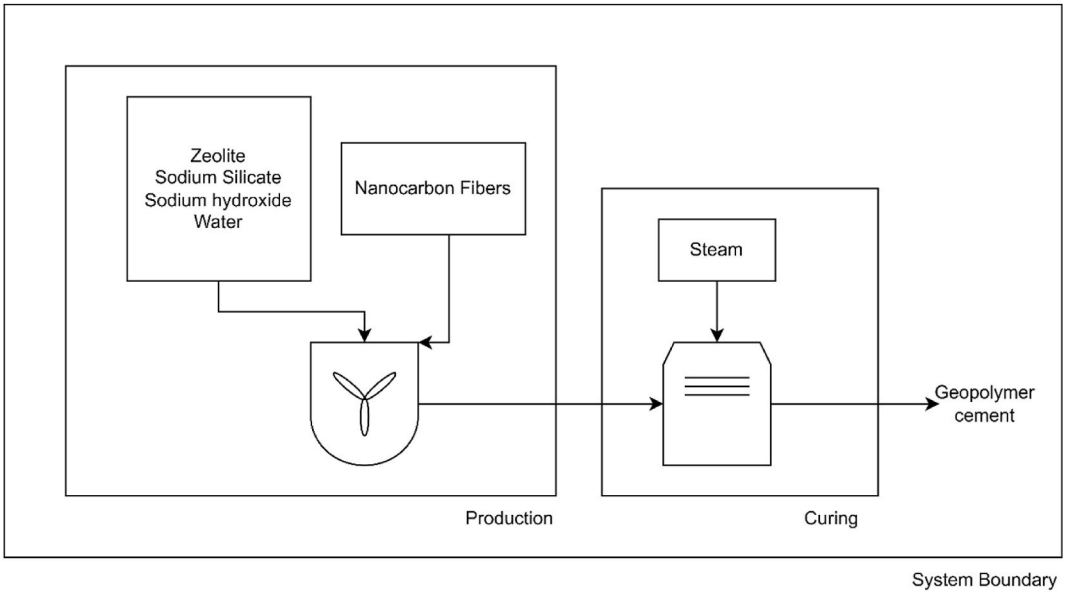

Fig. 4. System Boundary for 1 m^3 of CNF-GP composite production.

Machine.

Bulk resistivity method [49] was used to calculate the electrical conductivity of G0, G1, G2, G3, G0*, G1*, G2*, and G3*. Two copper electrodes were located on the two opposite faces of the plaque, and a humid sponge was placed between the geopolymer cube and the electrode (Fig. S5 in the Supplementary Information File). The Megohmmeter/Insulation Tester Fluke 1550 B current travels along the sample, closing the circuit and measuring the electric resistance.

3. Results

3.1. Bulk density

Table 2 presents the bulk density of the CNF-reinforced geopolymer composites. The bulk density rose concurrently with the increase of CNF concentration with in the geopolymer matrix. The increase in bulk density can be attributed to the inclusion of the fibers in the geopolymer matrix [31,50]. Voids or pores are natural structural components formed due to the evaporation of water or particle size or raw materials in the geopolymer matrix that can restrict material density. CNFs can successfully permeate these voids due to their tiny size and flexibility, which can lower pore volume. The three-dimensional geopolymer matrix is strengthened by a network thanks to its high aspect ratio, making the matrix more compact. Furthermore, the robust interfacial contact between the geopolymer matrix and the CNFs may help improve the stress distribution, improving the material's overall density [33,51].

3.2. Compressive strength

The results of the compressive strength tests of the geopolymer samples aged for 83 days of the curation process can be seen in Fig. 5. The strength for reference samples (G0) and all the CNF-reinforced composites can be associated with the three-dimensional network structure formed in geopolymerization reaction [33,52,53].

The G2 sample, which contains 0.20 wt% of CNF, presented a better compressive strength, with an increase of about 29.5% compared to the reference sample, G0. The geopolymer with 0.32 wt% CNF (G3) shows only a 10% increase in compressive strength compared to G0. However, the data exhibits a high degree of variability from the mean. This may be caused, in contrast to what happens with G2, by a poor dispersion of the CNFs [33]. At higher concentrations, CNFs have the tendency to agglomerate, which

Table 2
The density of geopolymer samples of each series.

	Density (g/cm^3)			Average Density (g/cm^3)	Standard Deviation	Percentage Deviation (%)
	Sample 1	Sample 2	Sample 3			
G0	1.83	1.81	1.75	1.80	0.0432	2.41
G1	1.92	1.94	1.97	1.94	0.0232	1.19
G2	2.05	1.98	1.90	1.98	0.0790	4.00
G3	2.02	2.15	1.98	2.05	0.0932	4.55

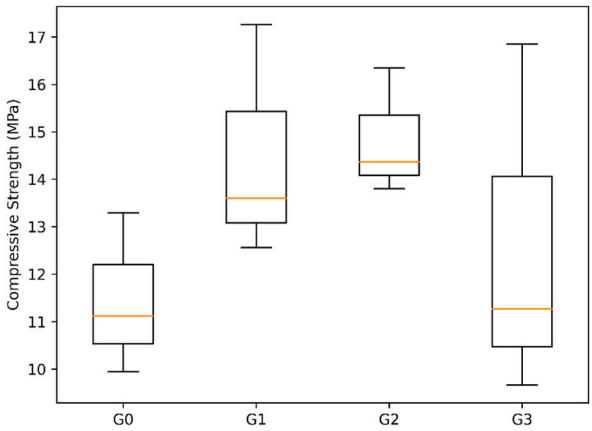

Fig. 5. Compressive strength tests of G0, G1, G2, and G3 samples cured for 83 days. The orange line represents the median value. (For interpretation of the references to color in this figure legend, the reader is referred to the Web version of this article.)

causes the formation of stress points where the forces can cause more damage instead of dispersing the applied force throughout the composite. These clusters do not allow for proper dispersion of the fibers in the matrix. These weak points cause a decrease in the overall compressive strength of the construction material. Some data exhibits higher compressive strength where the fibers in the sample may have rearranged properly. This hypothesis agrees with what is observed in the G3 sample and it is consistent with the existing literature, indicating a decline in resistance due to the agglomeration [12,33,48,54].

The addition of 0.07 and 0.2 wt% CNFs resulted in an enhanced compressive strength. This aligns with the phenomena explained by Da Luz et al. [12], which suggested that a decrease in the number of macropores upon the addition of CNTs was achieved [38]. This causes not only denser construction material, but an interaction between CNTs and the geopolymer matrix that successfully bridged the microcracks, improving its bonding behavior and strength.

3.3. TGA

Table 3 demonstrates the thermal stability of the geopolymer samples. A significant weight loss documented across all geopolymer samples is observed up to 200 °C. The weight loss resulted from the evaporation of the surface water (hydrates) and water within the pores of the geopolymer [8,55]. The second step in weight loss is observed between 200 and 600 °C, which is attributed to the dehydroxylation of Si–OH or Al–OH groups in the geopolymer structure. This variation exists since dehydroxylation is limited by some aspects, such as the physical arrangement, the displacement of the hydroxyl groups, and their reactivity [56]. Finally, between 600 and 800 °C, all geopolymer samples exhibited a minimal weight change since, at that temperature, the decomposition of carbonate species in geopolymers occurs [8,55].

The CNFs barely influence the loss of water in the range of 200–600 °C. This can be explained since the addition of CNTs makes the effect of pore-filling of the geopolymer matrix, including in the curation process, making the specimens more thermally stable, which can resist more in the water evaporation processes [33,51].

The TGA-DTA curves for G0, G1, G2, and G3 can be seen in Fig. 6. The thermograms between the G0-G3 and G0*-G3* samples are comparable (see Fig. S6 in the Supplementary Information File). The samples presented an endothermic process from room temperature (RT) to 100 °C [8]. Although a less intense endothermic peak was observed for the reference geopolymer (G0), less energy consumption and less matter were lost throughout the test. However, for G1, G2, and G3, the DSC curves increase, reach a peak, and decrease (Fig. 6). This can be attributed to the absence of CNFs in the G0 sample, making free water easier to evaporate. The second endothermic process above 400 °C is probably contributed by the condensation of Si–OH or Al–OH groups of the geopolymer, which agrees with several studies [8,57].

In conclusion, it can be affirmed that within the tested temperature range of 25–1000 °C, the TGA profiles exhibit a similar trend for the SiO_2/Na_2O ratios of 2.4. Notably, convergence is observed, especially for G0*, G1*, and G2*, up to 750 °C. The profile for the G3*

Table 3
Thermogravimetric analysis of zeolite and its corresponding geopolymers.

	Mass loss (%)								
Temperature (°C)	Zeolite	G0	G1	G2	G3	G0*	G1*	G2*	G3*
RT-200	4.95	8.79	9.10	8.92	8.88	10.12	10.64	11.54	11.47
200–400	1.95	2.28	2.53	2.60	2.66	2.93	2.89	2.53	2.41
400–600	1.34	1.12	1.13	1.18	1.41	1.14	1.15	1.02	0.91
600–800	0.39	0.24	0.44	0.44	0.60	2.02	1.32	1.03	0.90
RT-800	8.63	12.48	13.2	13.14	13.55	16.21	16.00	16.12	15.69

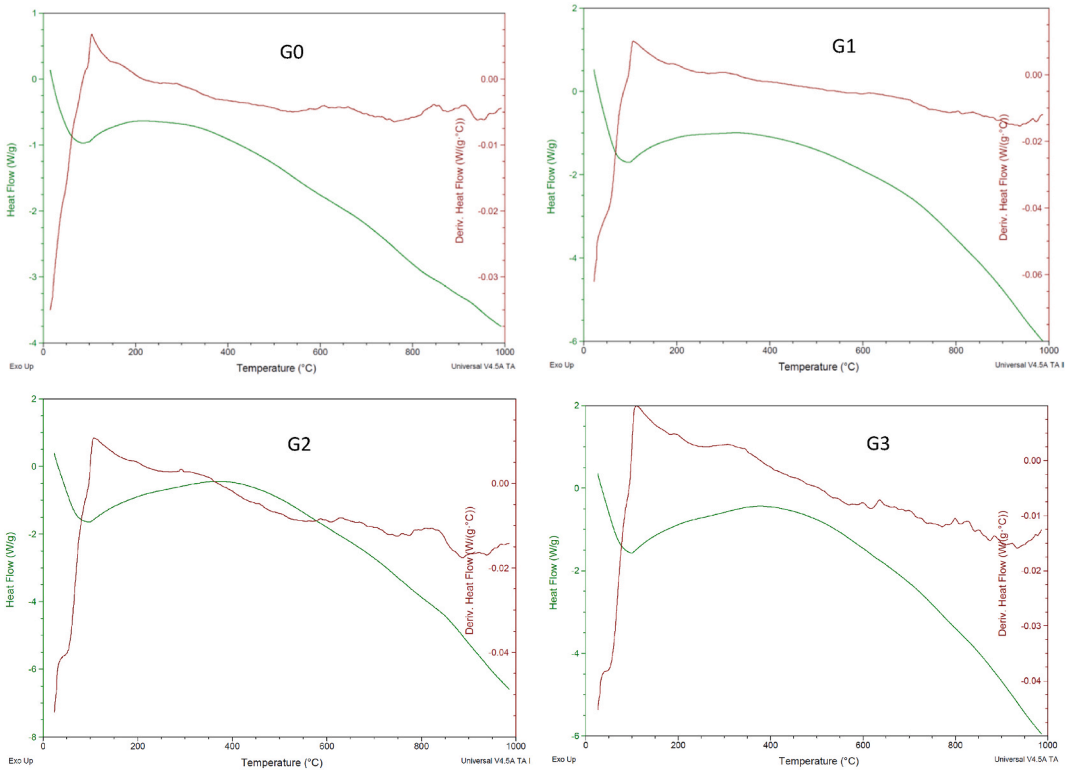

Fig. 6. Thermal phenomenon of G0, G1, G2, and G3 samples heated up to 1000 °C.

follows a very similar trend as the other, but it is of a lower magnitude for the entire tested temperature range. On the other hand, the TGA profiles for the SiO_2/Na_2O ratios of 3.4 do not closely align, and fluctuations occur at the lower temperatures tested. A notable divergence is observed around 700 °C, particularly for the G0 sample when compared to G1, G2, and G3.

3.4. FTIR spectral analysis

FTIR spectra, G0 (plain geopolymer), G1, G2, and G3 are shown in Fig. 7. Also, the spectra for G0*, G1*, G2*, and G3* are shown in Fig. S7. The peaks around 3446 cm^{-1} and 1640 cm^{-1} for all the samples are attributed to the stretching vibrations of the O–H group and the bending of free water absorbed [12,53]. Peaks between 1412 and 1424 cm^{-1} represent the stretching vibration of C–O of carbonates [12,51]. At this point, the effect on the concentration of CNFs is shown since a shift to the left occured in comparison with G0 (Fig. 7 and Fig. S7). This shift can be explained due to the van der Waals forces on the CNFs [58–60]. Peaks between 1029 and 1040 cm^{-1} represent asymmetric stretching vibration of T-O-Si (T = Si or Al) [12,51]. Peaks between 800 and 797 cm^{-1} represent symmetric stretching vibration of (Si–O) [61] attributed to quartz [51]. Peaks between 693 and 695 cm^{-1} are related to the symmetric stretching vibration of Si–O–Si [12,51]. The 580-588 cm^{-1} peaks represent Si–O–AlVI, where aluminum is in octahedral coordination [33,51,62]. Peaks between 521 and 530 cm^{-1} represent Si–O–Si bending vibrations [12].

A subtle difference in the FTIR spectrum of the reference geopolymer, G0, concerning the CNF-geopolymers is shown in peaks

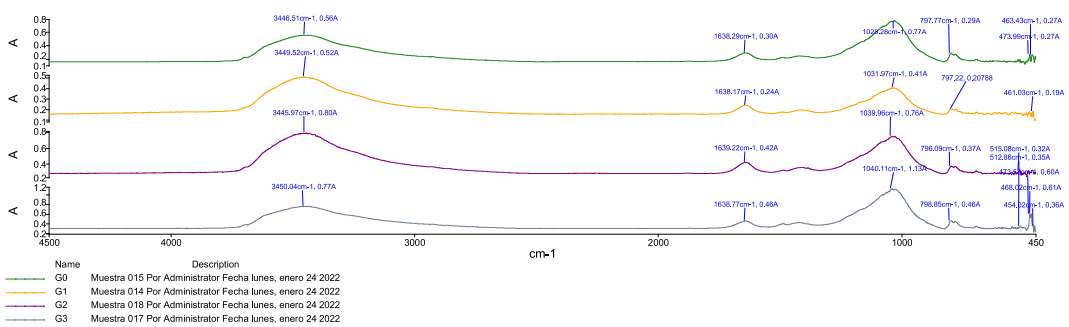

Fig. 7. FTIR spectra for G0, G1, G2, and G3 correspond to 0.000%, 0.07%, 0.12%, and 0.32% of CNF in geopolymer by weight.

between 467 and 461 $cm^{-1,}$ representing O–Si–O bending vibrations [12]. The reference geopolymer presents the peak at 467 cm^{-1}; meanwhile, the CNF-geopolymers are present at 461 cm^{-1} at a lower frequency. Since an FTIR band results from a non-zero dipole moment, a weaker band would suggest a near-perfect molecular geometry and crystallinity of the material components present in the sample [63]. This phenomenon is explained by Bi et al. [64] as due to the interfacial or van der Waals interactions, a cohesive interaction.

3.5. X-ray diffraction analysis

The XRD diffractogram of G0, G1, G2, and G3 are shown in Fig. 8 (crystalline phases: Mor: mordenite (Zeolite), and Qz: Quartz). The geopolymers comprise 12.3–18.4% quartz, 11.8–16.8% mordenite, 4.5–10.4% anorthite, and 54.9–68.3% amorphous (see Fig. 8). Similar behaviors are found across all the samples, with slightly more variation with samples Gi*(see Figs. S8 and S9 in the Supplementary Information File) since the changing of the molar composition of alkali-activated precursor can produce amorphous geopolymers [63]. Higher amorphous content was found in the geopolymer samples when compared to the zeolite raw material, which is related to a successful geopolymerization process, where the Si–O–Si of crystalline nature was open and reacted to form an amorphous network [63]. Additionally, no significant difference was found in the XRD G0, G1, G2, and G3 patterns, indicating that the CNFs do not contribute to the hydration, suggesting that no new strength-enhancing chemicals have been produced by CNFs in the geopolymer [63]. This outcome agrees with the findings reported by Azeem, Junaid, and Saleem [63].

3.6. Scanning electron microscopy

The presence of CNFs in the G2 and G3 geopolymer composite samples can be easily observed in scanning electron microscope images (see Fig. 9). The SEM image also shows a close-up view of a selected area of the G3 sample. Collected SEM images show agglomeration of the fibers through the sample, which may cause an effect on the variability of evaluated properties. For instance, better compressive strength and electrical conductivity can be seen in samples with good dispersion of the CNFs. Micropores and cracks can be seen through all the samples. Nevertheless, the samples that contain higher dosages of CNFs have larger pore sizes and cracks in the contact surface between the CNFs and geopolymer because of stress transferring between the matrix and filler [65]. However, it was seen that CNFs filled the gap or pores in the geopolymers. The CNFs detected and analyzed on the SEM image of the G3 sample in Fig. 9 show the dimensions and variability in the diameter from ~150 nm to 500 nm, which also affects compressive strength and conductivity data.

3.7. Electrical conductivity analysis

It was possible to obtain the samples' resistivity and conductivity (see Fig. 10) by measuring the electrical resistance. The resistivity is higher for the geopolymer G0 (183.77 kΩ•cm), and G0* (112.6 kΩ•cm) since they have a 0% of CNFs. From G0 to G1, there are almost 20 units of difference, and for G0* to approximately 12.5 units; this change is caused by the addition of CNFs as they can be conductive of electricity [66,67]. The electrical resistivity change could be explained by three potential mechanisms according to Zhou et al. [68]: the conductive percolation networks formed by embedded CNF, ions in the cement matrix's pore solution determine conductivity, and percolation due to the quantum tunneling effect.

The resistivity decreased for G2, however, G3 increases by almost seven resistivity units, obtaining 156.96 kΩ•cm; this may be caused by a poor dispersion of the fibers, as it is shown in Fig. 9. The latter could be explained by the fact that carbon nanomaterials tend to remain agglomerated because of the extremely strong van der Waals attractive forces, which can affect the performance of composites [60]. On the other hand, from G1* to G2*, the resistivity slightly increases and then decreases again for G3*, obtaining 111.87 kΩ•cm as the final measure. Yet, apparently, the geopolymers do not surpass the percolation threshold since the resistivity was

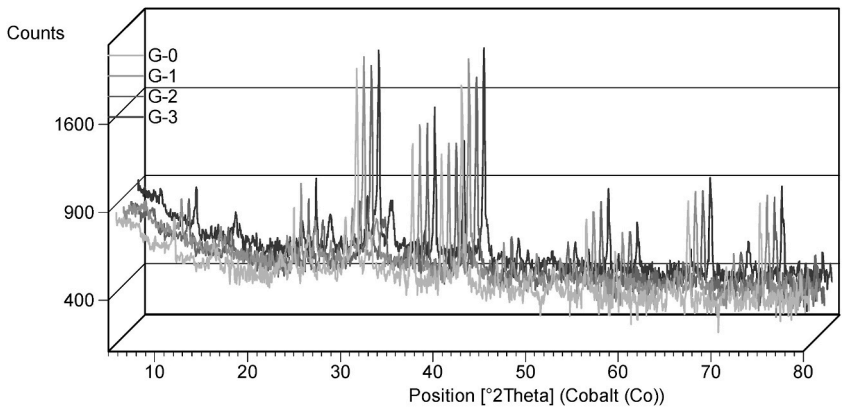

Fig. 8. XRD diffractogram for the G0, G1, G2, and G3.

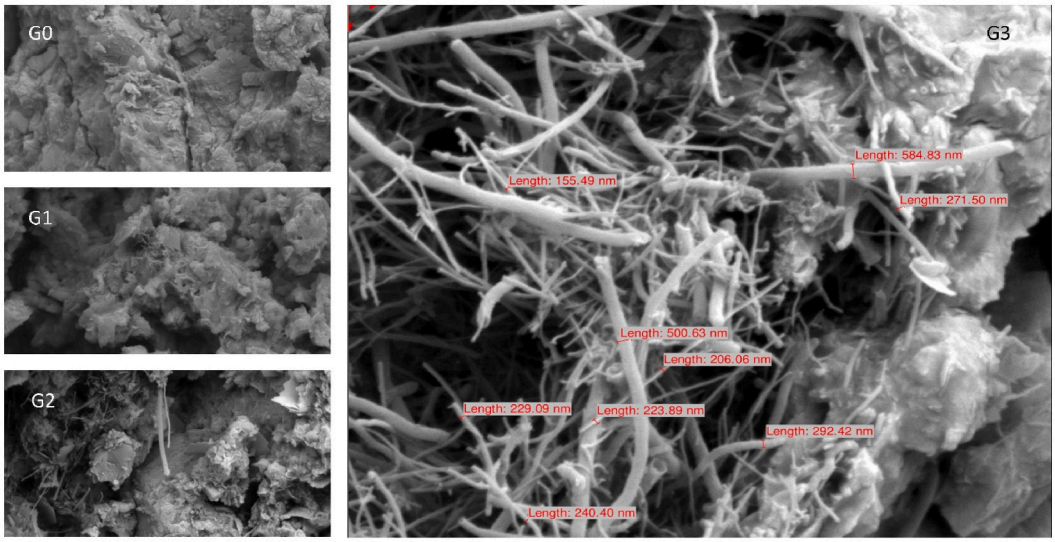

Fig. 9. SEM images at 10,000x and a scale of 10 μm for G0, G1, G2, and G3 samples.

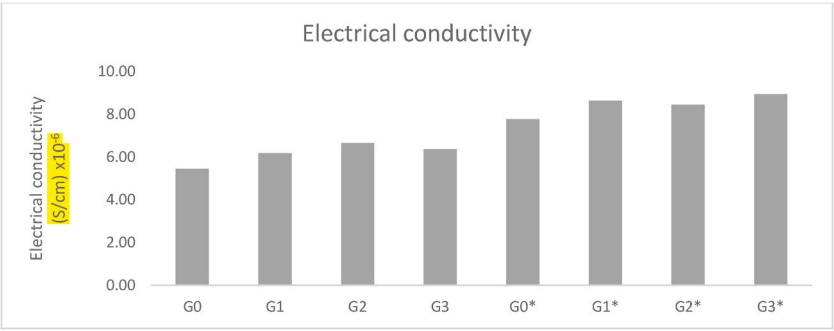

Fig. 10. Electrical conductivity of G0, G1, G2, G3, G0*, G1*, G2*, and G3* samples.

not reduced for several orders of magnitude [34]. For example, it was shown that cement-based composites may be employed as strain sensors by adding 1 and 1.15% vol. CNT [69] and resulting in a resistance of approximately 100 kΩ•cm, on the contrary, when adding 0.5% vol. CNT, the resistivity increased, hence 1% vol. could be the percolation threshold. Hence further investigation is needed to obtain the percolation threshold of CNFs embed in geopolymer.

Generally, electrical conductivity exhibits a slight increase when the CNFs percentage rises in the G0, G1, G2, and G3 geopolymers and the G0*, G1*, G2*, and G3*. The values between G0, G1, G2, and G3 geopolymers and the G0*, G1*, G2*, and G3* show a considerable difference since the second group has more sodium cations in the geopolymer, as the ratio of $SiO_2/Na_2O = 2.4$, meanwhile in the first group that ratio is 3.4.

In general, these results show congruency with the literature. For example, Hanjitsuwan et al. [70] evaluated the electric conductivities of geopolymers reinforced with CNTs made of different fly ash ratios and activator solutions between $5x10^{-4}$ and 10^{-3} S/cm. Also, Mizerová et al. [9] reported an electrical conductivity of $6.31x10^{-5}$S/cm using graphite powder in geopolymers. The results are slightly below the electrical conductivity shown in the literature, but this can be caused by the quantity of CNFs being very small compared to the percentages of CNTs in geopolymer. Improving the geopolymer's electrical conductivity is essential for piezoelectric, corrosion-resistant components, or other multipurpose applications. Conductive fillers made of structured carbon can help achieve this purpose [34].

3.8. Life cycle assessment

The life cycle assessment focused on the environmental impact of the production of carbon nanofibers, zeolite, and alkaline activators that form the geopolymer-CNF composite. Global warming potential has been especially evaluated as it is one of the foremost parameters to assess the performance of the composites because of the significant contribution of CO_2 from ordinary Portland cement (OPC).

Temizel-Sekeryan et al. [44] extensively reviewed different routes for multiwall CNT (MWCNTs) production. Three raw materials (Acetylene, benzene, or toluene) with their respective production schemes were compared based on reported routes. Fig. 11 shows the normalized results for the three options analyzed: acetylene in blue, benzene in orange, and toluene in green color. Toluene hydrocarbon gas and its production are the options that have a higher impact in the analyzed categories. In comparison, benzene shows the best environmental performance for climate change, acidification, and eutrophication, among other categories. For this reason, the source for CNFs was benzene because it would add less impact to our geopolymer composite. Studies show that benzene is the carbon source for CNFs with less impact on global warming indicators, and it can be further reduced by the source of electricity used (i.e., wind, solar, hydro, etc.) [44]. Even though benzene is a known carcinogenic substance, its process has less impact on the human carcinogenic category as it not only weights the use of the hydrocarbon source but other reagents used and energy consumed. For instance, the toluene process consumes about 79 kg of HCl per kg of MWCNT, but the benzene process only consumes 19 kg of H_2SO_4.

Table 4 shows the characterized impact results for the geopolymer cement mixes incorporating CNFs using benzene as a carbon source. In the global warming category, there is a maximum difference of 43% between the conventional geopolymer (G0) and the composite with a higher proportion of CNFs (G3) in terms of kilograms of CO_2 equivalent. In the same way, the acidification potential or terrestrial acidification category has a difference of 46%. The differences between the geopolymer with no CNFs and the ones with fibers in the other categories do not exceed 45%.

Normalizing these categories will allow for a more accurate comparison of the results between each mix. In this matter, the evaluation of the environmental performance of the best alternative can be made with the notion of different parameters considered all at once (all impact indicators). Fig. 12 demonstrates a tendency between the addition of CNFs and the increase of the impact score across all impact categories assessed. The G1 mix, which comprises 0.07% fibers, gets the best environmental score among the three alternatives that incorporate CNFs, according to the LCA methodology.

Studies have evaluated the effect of adding CNFs/CNTs to cement/concrete composites, resulting in a lower carbon footprint [27]. However, geopolymers are already an alternative with considerably lower CO_2 emissions than OPC. For this reason, the effect of the inclusion of CNFs in the composite should keep the binder climate change indicator as low as the reference geopolymer. In this sense, the mechanical properties of the geopolymer can be enhanced while maintaining the sustainability of the alternative construction materials. This is noticeable in Fig. 12, where the indicators, specifically global warming, showed no more than a 0.5 increase between the reference geopolymer and the highest load of CNFs.

The G1 mix was assessed to evaluate the contributions from each component involved. Each reagent, material, or process can be improved to reduce environmental impact. A maximum of 10% contribution from CNF production can be seen across all impact categories (See Fig. 13). The mix's two major/prime contributors are sodium silicate and zeolite. For instance, the main potential contributors to global warming are zeolite, sodium silicate, and CNFs, with 45, 41, and 9%, respectively. Water, steam, and electricity use contribute less than 1%, which is almost negligible in the graph. One study showed that using sodium silicate as the activator contributes significantly [37] to environmental impacts, a range of 55–72%. For G1, the contribution of this sodium silicate has been reduced to approximately 25%. Further optimization that aims for environmental impact reduction could include using waste materials like ash or silica prepared from rice [71,72] as raw materials with less burden for the process.

Studies have shown that OPC cement constitutes 90% of the allocated environmental impacts on concrete mixtures, especially for the global warming category [73]. For this reason, most studies assess concretes instead of cementitious binders. The impact of the concrete is lower than pure cement as the latter is only partially used while adding coarse and fine aggregates [73,74]. However, geopolymer concrete, including coarse and fine aggregates, also results in lower global warming potential. For this reason, a geopolymer binder was evaluated in this study with the added carbon nanofibers to enhance thermomechanical properties such as thermal conductivity and compressive strength.

4. Conclusions

The current study evaluated the effect of CNFs integrated into a geopolymer matrix using zeolite as a base material, analyzed loading concentrations ranging from 0 to 0.32 wt%. The research assessed key properties such as compressive strength, electrical conductivity, crystallinity, and environmental impact.

A crucial finding is that CNF concentration and the geopolymer's density follow an inverse relationship. A less dense, more water absorptive, and more electrically conductive geopolymer composite was obtained at higher CNFs loading. However, this correlation is not mirrored in the compressive strength which showed a peak at an optimal CNF concentration before reducing its resistance to compression. This indicates a critical threshold for CNF concentration in the composite since CNFs tend to be difficult to disperse, which could be a source of error in our outcome. The clustering of CNTs is extremely unfavorable. All the samples presented similar thermal behavior, showing thermal stability across the range of evaluation. This is particularly relevant for applications demanding consistent performance under varying thermal conditions.

The life cycle assessment in this study highlights that CNFs produced from benzene have a more favorable environmental profile. Nonetheless, the loading of CNFs increases the environmental impacts of the geopolymer. Thus, composites with lower carbon fiber dosages offer sustainable alternatives. The findings showed the importance of considering a trade-off between sustainability and mechanical/electrical properties. In addition, water glass and zeolite extraction are two main contributors that emerge as critical exploration areas of research.

In advancing the understanding of CNF-reinforced natural zeolite-based geopolymer composites, this study sheds light on the intricate balance between material properties and environmental considerations. Future research should optimize CNF concentration, find the percolation threshold, and improve dispersion for maximal mechanical strength without compromising sustainability, explore

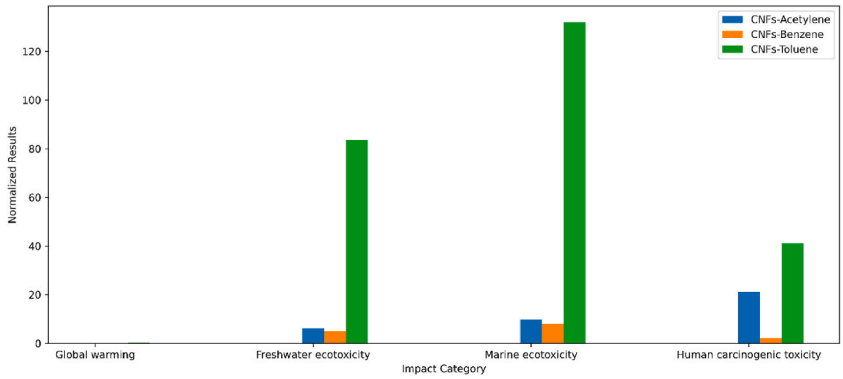

Fig. 11. Normalized results for 1 kg of CNF production based on different hydrocarbon sources.

Table 4
Characterized results for 1 m^3 of each of the geopolymer cement composites.

Impact Category	Unit	G0	G1	G2	G3
Global warming	kg CO_2 eq[a]	1,64E+03	1,80E+03	2,09E+03	2,36E+03
Terrestrial acidification	kg SO_2 eq[a]	7,67E+00	8,45E+00	9,87E+00	1,12E+01
Freshwater eutrophication	kg P eq[a]	1,12E+00	1,23E+00	1,42E+00	1,61E+00
Marine ecotoxicity	kg 1,4-DCB‣	1,06E+02	1,16E+02	1,33E+02	1,49E+02
Human carcinogenic toxicity	kg 1,4-DCB‣	6,93E+01	7,62E+01	8,88E+01	1,01E+02
Human non-carcinogenic toxicity	kg 1,4-DCB‣	2,34E+03	2,54E+03	2,89E+03	3,23E+03
Water consumption	m^3	6,84E+01	7,20E+01	7,82E+01	8,41E+01

[a] Eq: equivalent, ‣DCB: Dichlorobenzene.

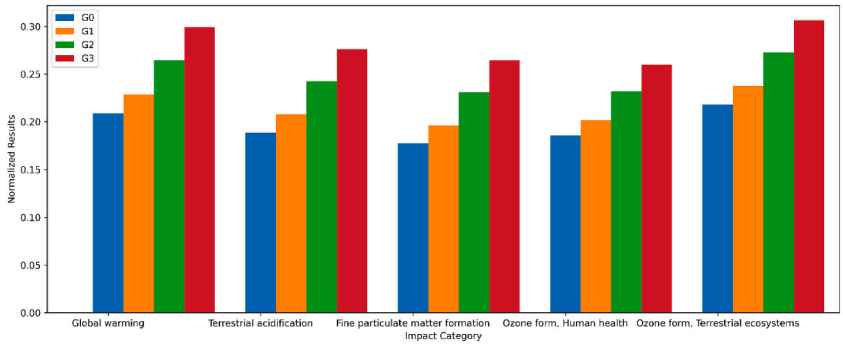

Fig. 12. Normalized results for the analyzed functional unit of the system.

alternative environmentally friendly CNF sources, and reduce the environmental impact of key components like water glass and zeolite. Such investigations will pave the way for developing more sustainable, high-performance geopolymer composites tailored for diverse applications.

Data availability statement

The data is available through the manuscript and in additional supplementary information file.

CRediT authorship contribution statement

Adriana Alvarado: Writing – original draft, Investigation, Data curation. **Haci Baykara:** Writing – review & editing, Supervision, Project administration, Methodology, Investigation, Formal analysis, Conceptualization. **Ariel Riofrio:** Writing – original draft, Software, Investigation, Formal analysis. **Mauricio Cornejo:** Writing – review & editing, Formal analysis. **Wilson Merchan-Merchan:** Writing – review & editing, Formal analysis.

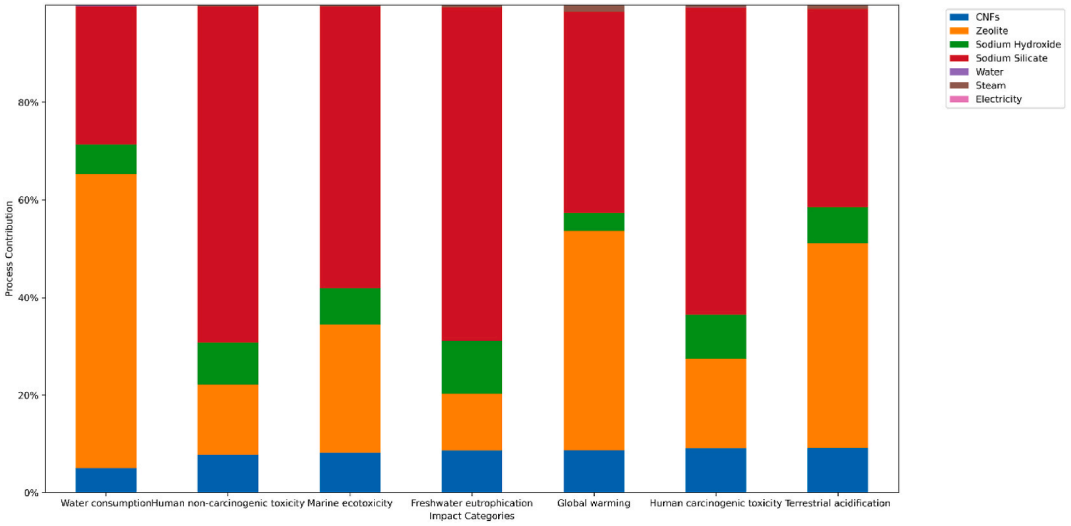

Fig. 13. Process contribution for the functional unit considered for G1 sample production.

Declaration of competing interest

The authors declare that they have no known competing financial interests or personal relationships that could have appeared to influence the work reported in this paper.

Acknowledgments

We want to thank Pré Consultants B.V. for providing the SimaPro software license for academic use and research. WMM would like to acknowledge the support of the Cluster SEED Funding by the School of Aerospace and Mechanical Engineering at the University of Oklahoma.

Appendix A. Supplementary data

Supplementary data to this article can be found online at https://doi.org/10.1016/j.heliyon.2024.e28079.

References

[1] B. Singh, G. Ishwarya, M. Gupta, S.K. Bhattacharyya, Geopolymer concrete: a review of some recent developments, Construct. Build. Mater. 85 (2015) 78–90, https://doi.org/10.1016/j.conbuildmat.2015.03.036.
[2] C. Li, S. Cui, Z. Nie, X. Gong, Z. Wang, N. Itsubo, The LCA of portland cement production in China, Int. J. Life Cycle Assess. 20 (2015) 117–127, https://doi.org/10.1007/S11367-014-0804-4/TABLES/5.
[3] Interternational Energy Agency (IEA), Technology Roadmap - Low-Carbon Transition in the Cement Industry, 2018, p. 66. Paris, https://www.iea.org/reports/technology-roadmap-low-carbon-transition-in-the-cement-industry.
[4] B.A. Tayeh, A.M. Zeyad, I.S. Agwa, M. Amin, Effect of elevated temperatures on mechanical properties of lightweight geopolymer concrete, Case Stud. Constr. Mater. 15 (2021) e00673, https://doi.org/10.1016/j.cscm.2021.e00673.
[5] Ch Panagiotopoulou, E. Kontori, Th Perraki, G. Kakali, Dissolution of aluminosilicate minerals and by-products in alkaline media, J. Mater. Sci. 42 (2007) 2967–2973, https://doi.org/10.1007/s10853-006-0531-8.
[6] M.M. Al Bakri Abdullah, H. Kamarudin, I. Khairul Nizar, M. Bnhussain, Y. Zarina, A.R. Rafiza, Correlation between Na2SiO3/NaOH ratio and fly ash/alkaline activator ratio to the strength of geopolymer, Adv. Mater. Res. (2012) 341–342, https://doi.org/10.4028/WWW.SCIENTIFIC.NET/AMR.341-342.189, 189–193.
[7] C. Pavon, M.V. Chan-Pavon, D.A. Mena-Romero, J.F. Escalante-Euán, M.D. Rodríguez-Martín, Contribución de las Prácticas Profesionales en la formación de los Estudiantes Contribution of the Internship in the Professional formation in the Students of Chemical Engineering Faculty at the 11 (2018) 53–62, https://doi.org/10.4067/S0718-50062018000100053.
[8] N.A. Ulloa, H. Baykara, M.H. Cornejo, A. Rigail, C. Paredes, J.L. Villalba, Application-oriented mix design optimization and characterization of zeolite-based geopolymer mortars, Construct. Build. Mater. 174 (2018) 138–149, https://doi.org/10.1016/J.CONBUILDMAT.2018.04.101.
[9] C. Mizerová, I. Kusák, P. Rovnaník, Electrical properties of fly ash geopolymer composites with graphite conductive admixtures, in: Acta Polytech CTU Proc, Czech Technical University in Prague, 2019, pp. 72–76, https://doi.org/10.14311/APP.2019.22.0072.
[10] M.F. Kai, L.W. Zhang, K.M. Liew, Carbon nanotube-geopolymer nanocomposites: a molecular dynamics study of the influence of interfacial chemical bonding upon the structural and mechanical properties, Carbon N Y 161 (2020) 772–783.
[11] M. Saafi, K. Andrew, P.L. Tang, D. McGhon, S. Taylor, M. Rahman, S. Yang, X. Zhou, Multifunctional properties of carbon nanotube/fly ash geopolymeric nanocomposites, Construct. Build. Mater. 49 (2013) 46–55, https://doi.org/10.1016/j.conbuildmat.2013.08.007.
[12] G. da Luz, P.J.P. Gleize, E.R. Batiston, F. Pelisser, Effect of pristine and functionalized carbon nanotubes on microstructural, rheological, and mechanical behaviors of metakaolin-based geopolymer, Cem. Concr. Compos. 104 (2019) 103332, https://doi.org/10.1016/j.cemconcomp.2019.05.015.

[13] K.A. Komnitsas, Potential of geopolymer technology towards green buildings and sustainable cities, Procedia Eng. 21 (2011) 1023–1032, https://doi.org/10.1016/j.proeng.2011.11.2108.

[14] J. Cai, J. Pan, X. Li, J. Tan, J. Li, Electrical resistivity of fly ash and metakaolin based geopolymers, Construct. Build. Mater. 234 (2020), https://doi.org/10.1016/j.conbuildmat.2019.117868.

[15] P. Payakaniti, S. Pinitsoonthorn, P. Thongbai, V. Amornkitbamrung, P. Chindaprasirt, Effects of carbon fiber on mechanical and electrical properties of fly ash geopolymer composite, Mater Today Proc 5 (2018) 14017–14025, https://doi.org/10.1016/j.matpr.2018.02.054.

[16] C. Luan, X. Shi, K. Zhang, N. Utashev, F. Yang, J. Dai, Q. Wang, A mix design method of fly ash geopolymer concrete based on factors analysis, Construct. Build. Mater. 272 (2021) 121612, https://doi.org/10.1016/J.CONBUILDMAT.2020.121612.

[17] N.B. Singh, B. Middendorf, Geopolymers as an alternative to Portland cement: an overview, Construct. Build. Mater. 237 (2020), https://doi.org/10.1016/j.conbuildmat.2019.117455.

[18] S.J. Wei, J.L. Tan, W.L. Lu, L.P. Liu, S.J. Yu, G.J. Zheng, Preparation and performances of geopolymer-based plant fiber composites, Solid State Phenom. 281 (2018) 266–271, https://doi.org/10.4028/www.scientific.net/SSP.281.266.

[19] T. Lingyu, H. Dongpo, Z. Jianing, W. Hongguang, Durability of geopolymers and geopolymer concretes: a review, Rev. Adv. Mater. Sci. 60 (2021) 1–14, https://doi.org/10.1515/rams-2021-0002.

[20] M. Khan, M. Shahzad, M.A. Basit, R.U. Din, S. Akhtar, S.W. Husain, R.E. Aune, A Comparative study of carbon nanotubes and graphene Nanoplatelets on structure-property relationship of Aluminium matrix composites Synthesized by Spark Plasma Sintering, Minerals, Metals and Materials Series (2022) 21–40, https://doi.org/10.1007/978-3-030-92567-3_2/COVER.

[21] M.A. Basit, S.E.A. Qais, M.S.U. Malik, G.U. Rehman, F.S. Awan, L.A. Khan, T. Subhani, Incorporation of carbon nanotubes on strategically de-sized carbon fibers for enhanced interlaminar shear strength of epoxy matrix composites, J. Chem. Soc. Pakistan 41 (2019) 655–663, https://doi.org/10.52568/000783/JCSP/41.04.2019.

[22] Y.A. Kim, T. Hayashi, M. Endo, M.S. Dresselhaus, Carbon nanofibers, Springer Handbook of Nanomaterials (2013) 233–262, https://doi.org/10.1007/978-3-642-20595-8_7/FIGURES/726.

[23] J. Liang, M.C. Saha, M.C. Altan, Effect of carbon nanofibers on thermal conductivity of carbon fiber reinforced composites, Procedia Eng. 56 (2013) 814–820, https://doi.org/10.1016/J.PROENG.2013.03.201.

[24] E. Hammel, X. Tang, M. Trampert, T. Schmitt, K. Mauthner, A. Eder, P. Pötschke, Carbon nanofibers for composite applications, Carbon N Y 42 (2004) 1153–1158, https://doi.org/10.1016/J.CARBON.2003.12.043.

[25] Y.K. Choi, Y. Gotoh, K.I. Sugimoto, S.M. Song, T. Yanagisawa, M. Endo, Processing and characterization of epoxy nanocomposites reinforced by cup-stacked carbon nanotubes, Polymer (Guildf) 46 (2005) 11489–11498, https://doi.org/10.1016/J.POLYMER.2005.10.028.

[26] Z. Wang, S. Wu, J. Wang, A. Yu, G. Wei, Carbon nanofiber-based functional nanomaterials for sensor applications, Nanomaterials 9 (2019), https://doi.org/10.3390/NANO9071045.

[27] K. Cui, D. Lu, T. Jiang, J. Zhang, Z. Jiang, G. Zhang, J. Chang, D. Lau, Understanding the role of carbon nanotubes in low carbon sulfoaluminate cement-based composite, J. Clean. Prod. 416 (2023) 137843, https://doi.org/10.1016/j.jclepro.2023.137843.

[28] S. Yan, F. Zhang, H. Li, B. Gao, P. Xing, P. He, D. Jia, Synthesis and mechanical properties of lightweight hybrid geopolymer foams reinforced with carbon nanotubes, Int. J. Appl. Ceram. Technol. 17 (2020) 2335–2345, https://doi.org/10.1111/IJAC.13543.

[29] P. Rovnaník, H. Šimonová, L. Topolář, P. Schmid, Z. Keršner, Effect of carbon nanotubes on the mechanical Fracture properties of fly ash geopolymer, Procedia Eng. 151 (2016) 321–328, https://doi.org/10.1016/J.PROENG.2016.07.360.

[30] A.-T. Akono, Fracture behavior of metakaolin-based geopolymer reinforced with carbon nanofibers, International Journal of Ceramic Engineering & Science 2 (2020) 234–242, https://doi.org/10.1002/CES2.10060.

[31] R. Zhang, S. Zhou, F. Li, Y. Bi, X. Zhu, Mechanical and microstructural characterization of carbon nanofiber–reinforced geopolymer nanocomposite based on Lunar Regolith Simulant, J. Mater. Civ. Eng. 34 (2022), https://doi.org/10.1061/(ASCE)MT.1943-5533.0004025.

[32] B. Maho, P. Sukontasukkul, G. Sua-Iam, M. Sappakittipakorn, D. Intarabut, C. Suksiripattanapong, P. Chindaprasirt, S. Limkatanyu, Mechanical properties and electrical resistivity of multiwall carbon nanotubes incorporated into high calcium fly ash geopolymer, Case Stud. Constr. Mater. 15 (2021) e00785, https://doi.org/10.1016/j.cscm.2021.e00785.

[33] S.M. Abbasi, H. Ahmadi, G. Khalaj, B. Ghasemi, Microstructure and mechanical properties of a metakaolinite-based geopolymer nanocomposite reinforced with carbon nanotubes, Ceram. Int. 42 (2016) 15171–15176, https://doi.org/10.1016/J.CERAMINT.2016.06.080.

[34] S. Zhang, N. Ukrainczyk, A. Zaoui, E. Koenders, Electrical conductivity of geopolymer-graphite composites: percolation, mesostructure and analytical modeling, Construct. Build. Mater. 411 (2024) 134536, https://doi.org/10.1016/J.CONBUILDMAT.2023.134536.

[35] X. Qian, H. Yang, J. Wang, Y. Fang, M. Li, Eco-friendly treatment of carbon nanofibers in cementitious materials for better performance, Case Stud. Constr. Mater. 16 (2022) e01126, https://doi.org/10.1016/j.cscm.2022.e01126.

[36] D.R. Vieira, J.L. Calmon, F.Z. Coelho, Life cycle assessment (LCA) applied to the manufacturing of common and ecological concrete: a review, Construct. Build. Mater. 124 (2016) 656–666, https://doi.org/10.1016/j.conbuildmat.2016.07.125.

[37] D.A. Salas, A.D. Ramirez, N. Ulloa, H. Baykara, A.J. Boero, Life cycle assessment of geopolymer concrete, Construct. Build. Mater. 190 (2018) 170–177, https://doi.org/10.1016/j.conbuildmat.2018.09.123.

[38] W. Wang, B. Wang, S. Zhang, Dispersion, properties, and mechanisms of nanotechnology-modified alkali-activated materials: a review, Renew. Sustain. Energy Rev. 192 (2024) 114215, https://doi.org/10.1016/J.RSER.2023.114215.

[39] ASTM International, Standard Test Method for Compressive Strength of Hydraulic Cement Mortars (Using 2-in, or [50-mm] Cube Specimens), Book of Standards Volume. 04.01 (2016). https://doi.org/10.1520/C0109_C0109M-16.

[40] B.V. Pré-Sustainability, SimaPro 9.3 (2022). https://simapro.com/.

[41] The International Standards Organisation, Environmental Management — Life Cycle Assessment — Principles and Framework, 2006. Standard No. 14040).

[42] G. Wernet, C. Bauer, B. Steubing, J. Reinhard, E. Moreno-Ruiz, B. Weidema, The ecoinvent database version 3 (part I): overview and methodology, Int. J. Life Cycle Assess. 21 (2016) 1218–1230, https://doi.org/10.1007/S11367-016-1087-8/FIGURES/7.

[43] A.D. Ramirez, A. Boero, B. Rivela, A.M. Melendres, S. Espinoza, D.A. Salas, Life cycle methods to analyze the environmental sustainability of electricity generation in Ecuador: is decarbonization the right path? Renew. Sustain. Energy Rev. 134 (2020) 110373 https://doi.org/10.1016/J.RSER.2020.110373.

[44] S. Temizel-Sekeryan, F. Wu, A.L. Hicks, Global scale life cycle environmental impacts of single- and multi-walled carbon nanotube synthesis processes, Int. J. Life Cycle Assess. 26 (2021) 656–672, https://doi.org/10.1007/s11367-020-01862-1.

[45] M. Goedkoop, R. Heijungs, A. De Schryver, J. Struijs, R. Van Zelm, ReCiPe 2008 A Life Cycle Impact Assessment Method Which Comprises Harmonised Category Indicators at the Midpoint and the Endpoint Level First Edition (Version 1.08) Report I: Characterisation Mark Huijbregts 3), 2013.

[46] M.A.J. Huijbregts, Z.J.N. Steinmann, P.M.F. Elshout, G. Stam, F. Verones, M. Vieira, M. Zijp, A. Hollander, R. van Zelm, ReCiPe2016: a harmonised life cycle impact assessment method at midpoint and endpoint level, Int. J. Life Cycle Assess. 22 (2017) 138–147, https://doi.org/10.1007/s11367-016-1246-y.

[47] H. Feng, J. Zhao, A. Hollberg, G. Habert, Where to focus? Developing a LCA impact category selection tool for manufacturers of building materials, J. Clean. Prod. 405 (2023) 136936, https://doi.org/10.1016/j.jclepro.2023.136936.

[48] P. Jittabut, S. Horpibulsuk, Physical and Microstructure properties of geopolymer nanocomposite reinforced with carbon nanotubes, Mater. Today Proc. 17 (2019) 1682–1692, https://doi.org/10.1016/J.MATPR.2019.06.199.

[49] P. Azarsa, R. Gupta, Electrical resistivity of concrete for durability evaluation: a review, Adv. Mater. Sci. Eng. 2017 (2017), https://doi.org/10.1155/2017/8453095.

[50] S. Yan, F. Zhang, J. Kong, B. Wang, H. Li, Y. Yang, P. Xing, Mechanical properties of geopolymer composite foams reinforced with carbon nanofibers via modified hydrogen peroxide method, Mater. Chem. Phys. 253 (2020) 123258, https://doi.org/10.1016/j.matchemphys.2020.123258.

[51] H.M. Khater, H.A. Abd El Gawaad, Characterization of alkali activated geopolymer mortar doped with MWCNT, Construct. Build. Mater. 102 (2016) 329–337, https://doi.org/10.1016/J.CONBUILDMAT.2015.10.121.

[52] C. Ferone, F. Colangelo, G. Roviello, D. Asprone, C. Menna, A. Balsamo, A. Prota, R. Cioffi, G. Manfredi, Application-Oriented chemical optimization of a metakaolin based geopolymer, Materials 6 (2013) 1920–1939, https://doi.org/10.3390/MA6051920, 6 (2013) 1920–1939.
[53] M.A. Soleimani, R. Naghizadeh, A.R. Mirhabibi, F. Golestanifard, Effect of calcination temperature of the kaolin and molar Na2O/SiO2 activator ratio on physical and microstructural properties of metakaolin based geopolymers, Iranian Journal of Materials Science and Engineering 9 (2012) 43–51.
[54] S.S. Kantak, K.J. Sullivan, B.E. Fisher, B.J. Knowlton, C.J. Winstein, Neural substrates of motor memory consolidation depend on practice structure, Nat. Neurosci. 13 (2010) 923–925, https://doi.org/10.1038/nn.2596.
[55] A. Nikolov, I. Rostovsky, H. Nugteren, Geopolymer materials based on natural zeolite, Case Stud. Constr. Mater. 6 (2017) 198–205, https://doi.org/10.1016/J.CSCM.2017.03.001.
[56] P. Duxson, G.C. Lukey, J.S.J. Van Deventer, Physical evolution of Na-geopolymer derived from metakaolin up to 1000 °c, J. Mater. Sci. 42 (2007) 3044–3054, https://doi.org/10.1007/S10853-006-0535-4/FIGURES/12.
[57] M.A. Villaquirán-Caicedo, R.M. de Gutiérrez, S. Sulekar, C. Davis, J.C. Nino, Thermal properties of novel binary geopolymers based on metakaolin and alternative silica sources, Appl. Clay Sci. 118 (2015) 276–282, https://doi.org/10.1016/J.CLAY.2015.10.005.
[58] H. Hu, Y. Liu, High modulus, high tenacity yarns, in: Technical Textile Yarns, Woodhead Publishing, 2010, pp. 329–386, https://doi.org/10.1533/9781845699475.2.329.
[59] V.V. Smirnov, L.I. Manevitch, Carbon nanotubes in arrays: competition of van-der-Waals and elastic forces, Dokl. Phys. 64 (2019) 218–221, https://doi.org/10.1134/S1028335819050070/FIGURES/4.
[60] W. Sekkal, A. Zaoui, High strength metakaolin-based geopolymer reinforced by pristine and covalent functionalized carbon nanotubes, Construct. Build. Mater. 327 (2022) 126910, https://doi.org/10.1016/J.CONBUILDMAT.2022.126910.
[61] A.S. De Vargas, D.C.C. Dal Molin, A.B. Masuero, A.C.F. Vilela, J. Castro-Gomes, R.M. Gutierrez, Strength development of alkali-activated fly ash produced with combined NaOH and Ca(OH)2 activators, Cem. Concr. Compos. 53 (2014) 341–349, https://doi.org/10.1016/j.cemconcomp.2014.06.012.
[62] C.Y. Heah, H. Kamarudin, A.M. Mustafa Al Bakri, M. Bnhussain, M. Luqman, I. Khairul Nizar, C.M. Ruzaidi, Y.M. Liew, Study on solids-to-liquid and alkaline activator ratios on kaolin-based geopolymers, Construct. Build. Mater. 35 (2012) 912–922, https://doi.org/10.1016/J.CONBUILDMAT.2012.04.102.
[63] M. Azeem, M.T. Junaid, M.A. Saleem, Correlated strength enhancement mechanisms in carbon nanotube based geopolymer and OPC binders, Construct. Build. Mater. 305 (2021) 124748, https://doi.org/10.1016/j.conbuildmat.2021.124748.
[64] S. Bi, M. Liu, J. Shen, X.M. Hu, L. Zhang, Ultrahigh self-sensing performance of geopolymer nanocomposites via unique interface engineering, ACS Appl. Mater. Interfaces 9 (2017) 12851–12858, https://doi.org/10.1021/ACSAMI.7B00419.
[65] X. Zhu, C. Lu, W. Li, S. Zhou, F. Li, J. Xiao, S.P. Shah, Effects of carbon nanofibers on hydration and geopolymerization of low and high-calcium geopolymers, Cem. Concr. Compos. 133 (2022) 104695, https://doi.org/10.1016/j.cemconcomp.2022.104695.
[66] K.M. Liew, M.F. Kai, L.W. Zhang, Carbon nanotube reinforced cementitious composites: an overview, Compos Part A Appl Sci Manuf 91 (2016) 301–323, https://doi.org/10.1016/J.COMPOSITESA.2016.10.020.
[67] S.K. Pillalamarri, F.D. Blum, A.T. Tokuhiro, M.F. Bertino, One-pot synthesis of Polyaniline−Metal nanocomposites, Chem. Mater. 17 (2005) 5941–5944, https://doi.org/10.1021/CM050827Y.
[68] Z. Zhou, N. Xie, X. Cheng, L. Feng, P. Hou, S. Huang, Z. Zhou, Electrical properties of low dosage carbon nanofiber/cement composite: percolation behavior and polarization effect, Cem. Concr. Compos. 109 (2020) 103539, https://doi.org/10.1016/J.CEMCONCOMP.2020.103539.
[69] D.Y. Yoo, I. You, S.J. Lee, Electrical properties of cement-based composites with carbon nanotubes, graphene, and graphite nanofibers, Sensors 17 (2017) 1064, https://doi.org/10.3390/S17051064, 17 (2017) 1064.
[70] S. Hanjitsuwan, P. Chindaprasirt, K. Pimraksa, Electrical conductivity and dielectric property of fly ash geopolymer pastes, Int. J. Miner. Metall. Mater. 18 (2011) 94–99, https://doi.org/10.1007/S12613-011-0406-0, 1 18 (2011.
[71] S.K.S. Hossain, L. Mathur, P.K. Roy, Rice husk/rice husk ash as an alternative source of silica in ceramics: a review, Journal of Asian Ceramic Societies 6 (2018) 299–313, https://doi.org/10.1080/21870764.2018.1539210.
[72] L. Caldas, D. Pinheiro, R.M. Sposto, L. Rosse Caldas, M. Leoni Martins Nascimento, D. Gabriel Lima Pinheiro, R. Maria Sposto, Literature review of life cycle assessment applied to green concretes, in: Proceedings of the 6th Amazon & Pacific Green Materials Congress and Sustainable Construction Materials, LAT-RILEM Conference, Cali, 2016.
[73] S.H. Teh, T. Wiedmann, A. Castel, J. de Burgh, Hybrid life cycle assessment of greenhouse gas emissions from cement, concrete and geopolymer concrete in Australia, J. Clean. Prod. 152 (2017) 312–320, https://doi.org/10.1016/j.jclepro.2017.03.122.
[74] M. Rabie, M.R. Irshidat, N. Al-Nuaimi, Ambient and heat-cured geopolymer composites: mix design optimization and life cycle assessment, Sustainability 14 (2022) 4942, https://doi.org/10.3390/SU14094942, 14 (2022) 4942.
[75] J. Davidovits, Geopolymers and geopolymeric materials, Journal of Thermal Analysis 35 (1989) 429–441, https://doi.org/10.1007/BF01904446.